 doi:10.20944/preprints202010.0351.v1

Article

In silico selection and *in vitro* evaluation of novel inhibitors of *Streptococcus mutans* Ag I/II surface protein

Raúl E. Rivera-Quiroga[1,2*], Néstor Cardona[1], Leonardo Padilla[2], Wbeimar Rivera[3], Cristian Rocha-Roa[4], Mayri A. Diaz De Rienzo [5], Sandra M. Morales[3], María C. Martinez[3]

[1] Faculty of dentistry, Antonio Nariño University. Group of Investigation in oral Health. Av. Bolívar # 49 North – 30, Armenia – Quindío (Zip Code: 630001), Colombia; Raul Eduardo Rivera - rriveraquiroga@uan.edu.co. Nestor Ivan Cardona - nestorcardonape@uan.edu.co.

[2] Faculty of Health Sciences, Quindío University, GYMOL Group street 12N, Armenia, Quindío (Zip Code: 630001), Colombia. lpadilla@uniquindio.edu.co

[3] Faculty of Dentistry, University of Antioquia, Oral Microbiology Laboratory, 64 Street No. 52-59, Block 31, No. 216, Health Area, Medellin – Antioquia (Zip Code: 050001) Colombia. Wbeimar Rivera - wbeimar.rivera@udea.edu.co. Sandra Milena Morales - sandra.morales@udea.edu.co. Maria Cecilia Martinez - mcecilia.martinez@udea.edu.co.

[4] Faculty of Health Sciences, Quindío University, GEPAMOL Group street 12N, Armenia, Quindío (Zip Code: 630001), Colombia. ccrochar@uqvirtual.edu.co.

[5] School of Pharmacy and Biomolecular Sciences, Liverpool John Moores University, James Parsons Building 10.05C, Byrom Street, Liverpool (Zip Code: L3 3AF), United Kingdom. m.a.diaz@ljmu.ac.uk.

* Correspondence: Raul Eduardo Rivera Quiroga, Group of Investigation in Oral Health, Faculty of Dentistry, Antonio Nariño University, Av. Bolívar # 49 North-30, Armenia, Quindío 630001, Colombia. Tel/Fax: +573128693374/+5767494981, E-mail: rriveraquiroga@uan.edu.co.

Abstract: *Streptococcus mutans* is well known for having virulence factors associated with its cariogenic role, such as glucosyltransferases, which have been used as targets for the virtual screening of molecules with inhibitory capacity. The Antigen I/II of *S. mutans* is involved in the adhesion to the surface of the tooth and the bacterial co-aggregation in the biofilm formation, despite that, this protein has not been used as a target in a virtual strategy search for inhibitors. In this study we identified *in silico* and evaluated *in vitro* molecules with adhesion inhibitory potential on *S. mutans* Ag I/II. A virtual screening of 883,551 molecules was conducted, cytotoxicity analysis on fibroblast cells, *S. mutans* adhesion studies, scanning electron microscopy analysis for bacterial integrity, and molecular dynamics simulation were also performed. We have found three molecules (ZI-187, ZI-939, ZI-906) that were not cytotoxic and inhibited the adhesion of *S. mutans* to polystyrene microplates. Molecular dynamic simulation by 300 nanoseconds showed stability of the interaction between ZI-187 and Ag I/II (PDB: 3IPK). This work provides three new molecules that targets Ag I/II and have the capacity to inhibit *in vitro* the *S. mutans* adhesion on polystyrene microplates and provides a new computational line for the search and selection of safe inhibitory molecules against different pathogens.

Key words: (*Streptococcus mutans,* adhesion proteins, Antigen I/II, Structure-based virtual screening, molecular dynamics)

Preprints (www.preprints.org) | NOT PEER-REVIEWED | Posted: 16 October 2020 doi:10.20944/preprints202010.0351.v1

1. Introduction

In 2016 dental caries was classified as the most prevalent pathology in the world, affecting 2.4 billion people [1,2]. This pathology is one of the oral diseases related to the oral microbiota alteration [3], characterized by perforations or structural damage of the teeth, called carious lesions [4]. There are three well known risk factors for the development of caries: personal factors that are related to socioeconomic status i.e., dental insurance coverage, attitudes and knowledge about oral health and oral hygiene; oral environmental factors such as saliva, fluoride, chewing gum, pH, bacteria, calcium, phosphates and proteins; and factors that directly contribute to the development of caries, like, the tooth, diet (consumption of sugars), bacterial biofilms and time [5].

Oral microorganisms that cannot adhere to a surface are transported by salivary flow out of the mouth and into the digestive tract, but many oral bacteria possess mechanisms of adherence to solid surfaces (co-adhesion), such as coated teeth from salivary films, to squamous surfaces such as epithelial tissue or bacteria that are attached to the surface (co-aggregation) [6]. Ability to form biofilms is one of the main *S. mutans* characteristics and it has been shown to express virulence factors for biofilm development through two pathways, one dependent and the other independent of sucrose. In the presence of sucrose, cell wall-associated glycosyltransferases (Gtfs) mediate the tight binding of *S. mutans* to the tooth surface, synthesizing glucans that interact with surface-associated glycan-binding proteins (GBPs) to promote cell-cell aggregation. On the other hand, in the absence of sucrose, *S. mutans* synthesizes several important adhesins such as antigen I/II (also called SpaP, Pac), which specifically binds to a glycoprotein called SAG (salivary agglutinin) [7] which has been proposed that participate as well in the tooth bacterial adhesion, being fundamental for biofilm formation, due to its ability to promote the aggregation and invasion of the dentin of the collagen-dependent tooth [8,9].

Currently, to the best of our knowledge, there are not studies of molecules with an antibiofilm activity, which could prevent the formation of the cariogenic biofilm without affecting the normal oral microbiota. However, different strategies have been proposed, for example, molecules derived from natural products, metal ions and oxidizing agents and even antibodies that specifically bind to *S. mutans* targets (GtfB, GtfC, GtfD, Ag I/II) and inhibit their ability to develop biofilms [10,11]. In recent decades, the virtual search for inhibitors based on structures has taken interest in drug discovery [12–14]; for oral microbiology the use of this strategy is relatively new, particularly in the cariogenic context, but several proteins have been proposed that could be used as inhibitory molecules [15]. Gtf-C has been used as a target on the search of molecules with affinity to this protein and for selectively inhibition of *S. mutans* biofilms formation mainly due to the ability to inhibit the synthesis of expolysaccharides (EPS) *in vitro*, the biofilm formation and reduce *in vivo* the caries incidence and severity in a rat model [16,17]. Although the Ag I/II adhesin has been reported to play an important in the early stages of *S. mutans* biofilm development, participating in adhesion and co-aggregation with other bacteria and fungi such as *C. albicans*, there are no reports of computational studies that use this protein as target, therefore, the aim of this work is to identify *in silico* molecules with inhibitory effect on *S. mutans* Ag I/II, , which have no cytotoxic activity on human cells.

2. Results and Discussion

2.1. Structure based virtual Screening

2.1.1. Target proteins selection

The Ag I/II of *S. mutans* play an essential role in the etiology and pathogenesis of dental caries. Therefore, the discovery of inhibitors of Ag I/II may facilitate the development of drugs that prevent dental caries. Ag I/II is one of the cell wall-anchored adhesins that mediates attachment of *S. mutans* to tooth surfaces, recognize salivary glycoproteins, and are also involved in biofilm formation. Finding small-molecule that bind to the Ag I/II may interfere with the function of these adhesine. To

Preprints (www.preprints.org) | NOT PEER-REVIEWED | Posted: 16 October 2020 doi:10.20944/preprints202010.0351.v1

address this, we selected a sequence of the *S. mutans* Ag I/II adhesin and we found a crystal structure from different regions of AgI/II, which corresponds to the A3VP1 region (PDB: 3IPK) [18], C-terminal domain, region V (PDB: 1JMM) [19] and two from the C-terminal domain (PDB: 3QE5) [20] and (PDB: 3OPU) [21] (Figure S1). According to sequence similarity and coverage results (Table S1), the crystals structures of the proteins 3IPK and 3QE5 were selected, due to their role in *S. mutans* adhesion to the tooth, through their SAG binding [18] (Figure 1).

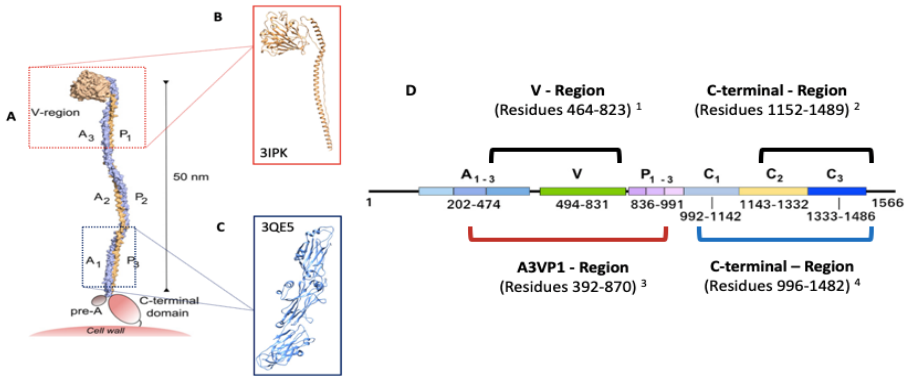

Figure 1. Crystals structures from the *S. mutans* Ag I/II protein (**A**). Model of *S. mutans* Ag I/II structure and predicted binding with human SAG (taken from [18]). (**B**) Crystal structure of A3VP1 protein from Ag I/II (3IPK) [18]. (**C**). Crystal structure C-domain protein from the Ag I/II (3QE5) [20]. (**D**). Schematic representation of the Ag I/II protein sequence (1566 aa) and the description of the aa residues that constitute the crystals structures of the protein regions: **1**- Region V (PDB: 1JMM) [19]; **2**- C-terminal domain [21]; **3**- A3VP1 region (PDB: 3IPK) [18] and **4**- the C-terminal region (PDB: 3QE5) [20].

Sequence and structural similarity analysis of 3IPK and 3QE5 was performed in order to identify other similar proteins that could be affected by the selected molecules. However, no significant homologies were found, which could be an indication that these molecules would not affect human (Table S2) or bacterial proteins important for the ecological balance of the oral microbiota. On the other hand, we have found sequence homologies with proteins from 23 bacterial species, which are mostly normal inhabitants of the oral cavity, gastrointestinal and genitourinary tracts, but are associated with different pathologies (Table S3, S4). Regarding the structural homologies for 3IPK and 3QE5 proteins, there were no similarities with any human or bacterial proteins, only with *S. mutans* Ag I/II regions, A3VP1 region (PDB: 3ioxA) [18] and N-terminal and C-terminal interaction complex (PDB: 4tshA) (Table S5) [26].

A fundamental step for the search of molecules based on virtual structures, is the pocket selection, these sites must have typical characteristics such as concave, have a variety of hydrogen bridge donors and acceptors and hydrophobic characteristics [27], otherwise, false negatives may occur when selecting molecules for *in vitro* assays, since errors may occur when there are no binding sites in the protein or when homology models are used, causing for example, small-volume pockets to be selected that will generate incorrect unions or conformations [28]. For that reason, in this study, two multiservers or specific programs were used for protein ligand binding site prediction, which have different selection algorithms, the MetaPocket uses a consensus method based on the predicted sites of four free access programs LIGSITEcs , PASS, Q-SiteFinder and SURFNET, which are combined to improve the success rate of the prediction and which is based on the geometry and surface of the proteins [29], unlike the COACH that uses the consensus of two methods, one based on the comparison of specific binding substructures (TM-SITE) and the other on the alignment of the sequence profile (S-SITE), for predictions of binding sites based on known proteins [30] (Figure S2).

2.1.2. Molecules selection

Ten molecules were arbitrarily selected according to their molecular docking score and ten according to the number of pockets interaction. The lowest docking score indicates high affinity

Preprints (www.preprints.org) | NOT PEER-REVIEWED | Posted: 16 October 2020 doi:10.20944/preprints202010.0351.v1

between the molecule and the ligand. Therefore, molecules that interacted in several binding sites were selected, because those could have a greater coating of the target protein allowing the inhibition of the two important regions of Ag I/II involved in its adhesin function.

Table 1. Energy interaction data obtained from recoupling using Autodock Vina with an exhaustiveness of twenty for the 3IPK and 3QE5 proteins with the selected molecules, molecule libraries and number of pockets in which each molecule interacted. The molecule highlighted in black was the only one that interacted with high affinity in different sites in both 3IPK and 3QE5 proteins. COA: COACH program. MET: Metapocket 2.0 program. Values highlighted in light blue represent the lowest interaction energy values.

NUMBER OF MOLECULES INTERACTION POCKETS	MOLECULES	LIBRARY	3IPK						3QE5					
			P1		P2		P3		P1		P2		P3	
			COACH	MET	COACH	MET	COACH	MET	COACH	MET	COACH	MET	COACH	MET
Not applicable	ZINC68568370	NAT	-12,8	-12,8	-7,5	-9	-9,4	-10,9	-8,5	-8,8	-8,1	-8,9	-7,1	-7,7
	ZINC70669788	NAT	-11,4	-12,8	-7,5	-8,4	-8,7	-10,1	-7,9	-8,7	-7,7	-7,6	-7,6	-6,5
	ZINC70669789	NAT	-11,5	-12,7	-7,3	-8,3	-8,8	-9,8	-8,1	-9	-7,9	-7,8	-7,8	-6,3
	ZINC34257514	NAT	-12,6	-12,6	-6,7	-8,8	-7,7	-9,8	-6,9	-8,7	-6,8	-7,6	-6,7	-7,6
	ZINC04817561	NAT	-10,3	-12,4	-10,1	-8,3	-8,6	-12,4	-7,2	-9,2	-7,1	-7,9	-7,2	-7
	ZINC67912808	NAT	-12,3	-12,5	-8,2	-8,8	-8,4	-9,1	-7,6	-9,5	-7,6	-8,1	-7,1	-6,8
	ZINC70686498	NAT	-12,2	-12,2	-7,8	-8,2	-8	-9,9	-7,4	-8,1	-7,3	-9,6	-6,6	-7,1
	ZINC04015296	NAT	-11,7	-11,6	-8,4	-9,8	-9	-11,7	-9,3	-11,4	-7,5	-9,3	-7,4	-9,8
	ZINC08594547	LRG	-11,6	-11,7	-7,7	-8,5	-8,1	-11,4	-7,6	-8,6	-7,1	-8,2	-6,5	-8,3
12	ZINC00970517	SM	-9,4	-9,4	-9	-8,2	-7	-9	-6,7	-7,7	-6,3	-7,5	-5,9	-7,3
12	ZINC01033612	SM	-9,3	-9,5	-8,7	-7,7	-7,3	-9,4	-7,4	-7,8	-7	-8,1	-7,4	-7,5
12	ZINC08647964	SM	-9,7	-9,8	-9,4	-7,9	-7,4	-10,4	-6,9	-8,4	-6,8	-8,7	-6,2	-7,5
12	ZINC12369546	SM	-9,5	-10	-9,1	-8,3	-7,5	-9,8	-7,9	-8,3	-6,7	-7,8	-6,8	-8,5
12	ZINC19924906	SM	-11,1	-11	-7,2	-8,2	-7,1	-9,2	-6,9	-8,3	-6,7	-7,5	-6,8	-7,5
12	ZINC03120327	SM	-9,6	-9,7	-10,1	-7,9	-7,1	-10,1	-6,7	-8	-7,1	-8	-6,9	-8,5
12	ZINC19835160	SM	-10,3	-9,5	-6,9	-8,7	-7,7	-9,7	-6,6	-8,4	-6,7	-8	-5,8	-6,9
12	ZINC19835187	SM	-10,7	-10,7	-9,2	-8,8	-8,5	-10,3	-8,1	-8,7	-7,5	-8,4	-6,9	-8,8
12	ZINC19924939	SM	-10,4	-10,4	-9	-8,9	-7,2	-8,1	-7,6	-7,5	-7,1	-8	-6,4	-7,9
12	ZINC59608258	SM	-9,4	-10,1	-7,8	-7,9	-7,2	-8,9	-6,8	-7,7	-6,1	-7,6	-6,3	-6,7

Once the selected molecules were reviewed, the molecules ZINC19924906 from the "Small" library was selected for both characteristics, obtaining in this step nineteen molecules, those with the lowest interaction energies, were molecules from the "Natural" library, such as ZINC68568370 with docking score -12.8. Molecules that had a greater number of binding sites, they were from the "Small" library and were coupled to the 12 pockets used for docking, meaning that they have affinity for both proteins 3IPK and 3QE5 (Table 1).

Molecules that comply the standard physical-chemical parameters and pharmacokinetic profiles are presented in table S6. However, one molecule was discarded for having an LD50 = 10mg / kg (C-II) (Figure S3) and fourteen for having the probability of presenting hepatotoxicity, carcinogenicity, immunotoxicity and/or mutagenicity characteristics (Figure S4). Finally, we obtained four molecules ZINC19835187 (ZI-187), ZINC19924939 (ZI-939), ZINC19924906 (ZI-906) and ZINC70686498 (ZI-498) (Figure 2) which did not present any probability of cytotoxic characteristics, as well as the Chlorhexidine (Figure S4).

Preprints (www.preprints.org) | NOT PEER-REVIEWED | Posted: 16 October 2020 doi:10.20944/preprints202010.0351.v1

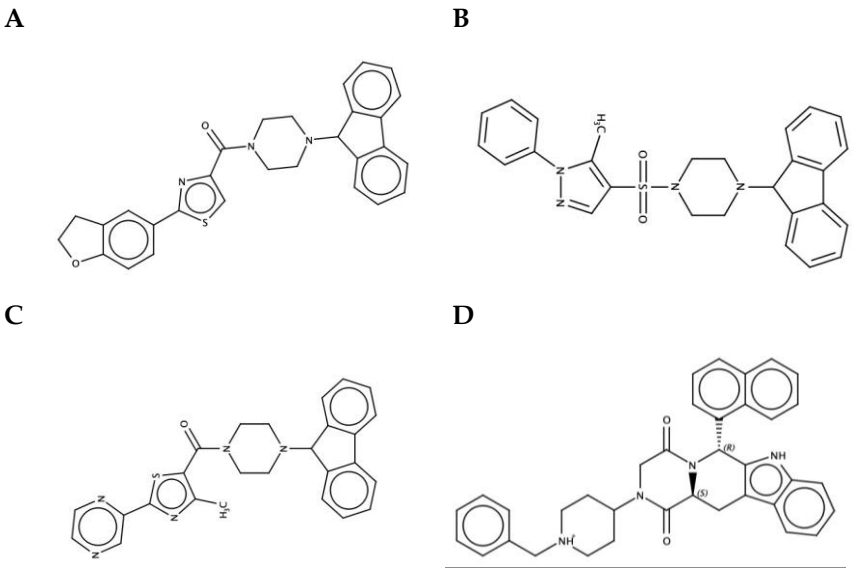

Figure 2. Molecules structures selected by *in silico* analysis, which have affinity for Ag I/II and inhibitory potential of *S. mutans* adhesion. **A**- ZI-187; **B**- ZI-939; **C**- ZI-906; **D**- ZI-498.

2.1.3 Molecule - protein interaction and solubility analysis

The presence of one or two hydrogen bridges was confirmed (Table S7) using the interaction complexes in the pockets established by the two predictors between the selected molecules and the 3IPK and 3QE5 proteins. This finding could indicate that the interaction between each molecules ZI-187, ZI-939 and ZI-906 with both proteins, would have very stable couplings, resulting in a possible inhibition of the *S. mutans* adhesion, since it has been shown that hydrogen bridges regulate and facilitate molecular interactions [31–35]. In addition, water solubility analysis of the molecules was conducted using a consensus from 3 methods resulting in a low aqueous solubility of the molecules (Table S8).

2.2 *In vitro* assays

2.2.1 Cytotoxicity and antimicrobial assays

It was found that molecules at concentrations of 100 µM have no effect on periodontal ligament fibroblast cells growth and the cells treated with molecules ZI-187 (P= 0.7372), ZI-939 (P= 0.8) and ZI-906 (P= 0.7964) (Figure S5). However, cells treated with each molecules showed changes in size and granularity. Therefore, it is important to analyze other human cell lines and add complementary analysis such as incorporation of DIOC6 for the mitochondrial membrane potential measurement [36] or apoptosis tests as Annexin V [37]. In addition, for antimicrobial assays molecules at concentrations of 1000 - 100 - 10 µM co-cultured experiments with *S. mutans* LT-11 or *C. albicans* - NCPF 3179, did not affect their growth (P= <0.001) (Figure S6 and S7, respectively).

2.2.2 Adhesion assays

It was established that treating *S. mutans* LT11 cells for three hours with all the molecules selected (ZI-187, ZI-939, ZI-906) inhibited the surface adhesion to a polystyrene microwell plate.

Preprints (www.preprints.org) | NOT PEER-REVIEWED | Posted: 16 October 2020 doi:10.20944/preprints202010.0351.v1

Inhibition with ZI-187 at a 25 µM was 32.8% (SEM = 2.1), at 50 µM it was 81.6% (SEM = 2.1), at 100 µM 95.0% (SEM = 0.6) and at 200 µM 95.9% (SEM = 0.6), with an IC50 of 27.6 µM (95% CI = 17,4 - 44,5) (Figure 3-A). Inhibition with ZI-939 molecules at a concentration of 25 µM was 48.6% (SEM = 7.6), at 50 µM 74.5% (SEM = 5.9), at 100 µM 83.1% (SEM = 5.5) and at 200 µM was 96.9% (SEM = 0.3), with an IC50 of 28.3 µM (95% IC = 20,2 – 39,8) (Figure 3-B) and for ZI- 906 at a concentration of 25 µM the inhibition was 17% (SEM = 3.3), at 50 µM 27.9% (SEM = 3.3), at 100 µM 81.7% (SEM = 1.8) and 200 µM was 93% (SEM = 0.7), with an IC50 of 59.5 µM (95% CI = 37,4 - 95,8) (Figure 3-C).

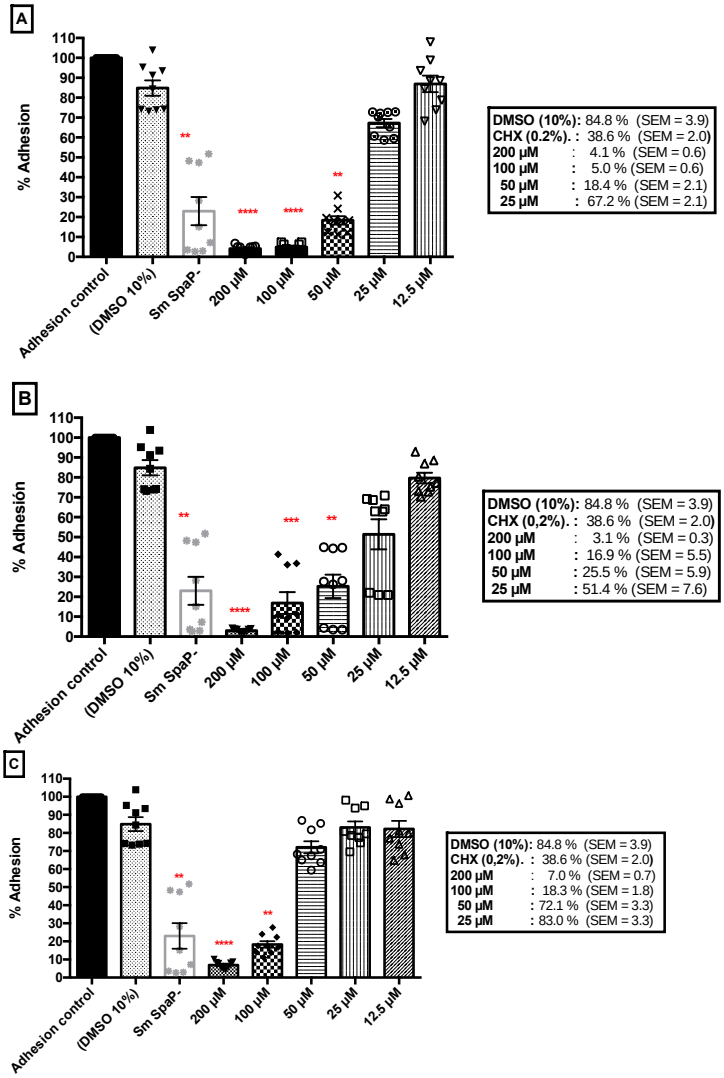

Figure 3. Surface adhesion of *S. mutans* - LT11 to a polystyrene microwell plate treated with molecules (A), ZI-939 (B) y ZI-906. The asterisks represent the level of significance.

Additionally, an agglutination phenomenon was observed when molecules with the bacteria was mixed, only at concentrations where the inhibition was affected (Figure 4). ZI-187 was the only molecule that maintained adhesion inhibition above 90% at a concentration of 100 µM, hence this was selected for scanning electron microscopy. Reduction of adherent bacteria was evident, and we did not observe morphological changes in *S. mutans* following treatment with ZI-187, bacteria had intact cell structure and round shapes with smooth edges (Figure 5).

Preprints (www.preprints.org) | NOT PEER-REVIEWED | Posted: 16 October 2020 doi:10.20944/preprints202010.0351.v1

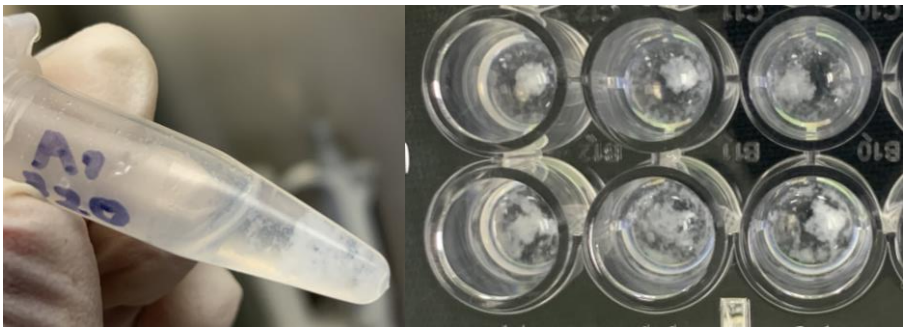

Figure 4. Photographic of the agglutination generated to the *S.mutans* - LT11 by adding any molecules ZI-187, ZI-939 or ZI-906 just in the concentrations where adhesion inhibition occurred.

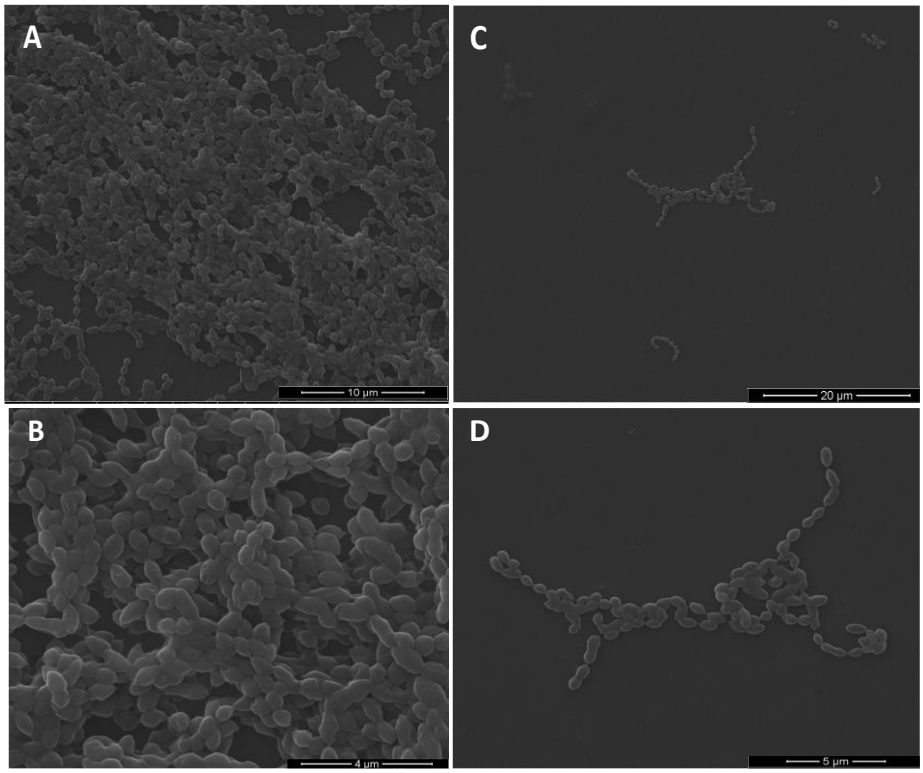

Figure 5. Scanning electron microscopy of S. mutans-LT11 surface adhesion to a polystyrene microwell plate. Without treatment at 7,000x (A) and 19,000x (B); and treated with 100 µM of molecule ZI-187, at of 4,000x (C) and 11,000x (D).

There are multiple chemical strategies that could limit the development of dental biofilm, however, most of them can have side effects on teeth, soft tissues or killing oral microbiota, which show the need for specific therapies for cariogenic bacteria. Several studies have focused on blocking two important mechanisms for *S. mutans* biofilm development, such as avoiding sucrose-dependent or sucrose-independent adhesion and interference of cellular signaling "Quorum sensing" [38]. This study was carried out avoiding the sucrose-independent adhesion way, which has been aimed mainly at blocking sortase A, a transpeptidase involved at the anchoring of cell surface proteins, including Ag I/II, through the LPXTG motif. It has been found that several molecules can reduce biofilm formation, through the inhibition of the sortase A [39,40], such is the case of the natural phenol curcumin, (*Curcuma longa*) with which it has been reported inhibition *S. mutans* sortase A activity with IC50: 10 µM and a MIC of 175 µM [41]. However, despite the multiple benefits of this molecule,

Preprints (www.preprints.org) | NOT PEER-REVIEWED | Posted: 16 October 2020 doi:10.20944/preprints202010.0351.v1

some toxic effects have also been evidenced related to the high doses as result from its use as a supplement in the diet [40,41]. Another natural product is named Morin, it has an inhibitory effect against *S. mutans* SrtA with IC50: 27.2 μM [42,43]. Morin other natural product, has an inhibitory effect against *S. mutans* SrtA with IC50: 27.2 μM [44], similar to the IC50 obtained with our molecules ZI-187 and ZI-939 (IC50: 27,6 y 28,3 μM, respectively). However, the antimicrobial activity of Morin has also been reported against *S. mutans* [45], differently from the molecules found in this study that did not present cytotoxic or antimicrobial activities.

2.2.3 Molecular dynamics simulations (MD)

Using molecular dynamics simulation, we have found that the complex 3IPK/ZI-187 attained a high stability after 300ns, during this time the 3IPK protein did not have strong changes when it was coupled with ZI-187 (Figure 6A), which could indicate that the interacting molecule moves on the pocket, but not drastically, this means that it does not destabilize the complex; in agreement with the RMSD result, no significant fluctuation of amino acid residues was observed, however, between residues 550-600 and 800-850, some differences were showed between the APO protein for 3IPK (black) and the complex (red) (Figure 6B), which could be due to the specific 3IPK residues that interact with ZI-187, since different types of interactions of ZI-187 with residues Leu 553 - Asp 554 - Thr 586 - Val 587 and Lys 811 - Lys 812 - Asn 814 - Ile 815 - Trp 816 were identified (Figure S8). In addition, 1 and 2 H-bonds were observed between the complex during the simulation time (Figure 6C) and a constant protein structure compactness in the complex (Figure 6D), these two parameters would support the stability of the interaction between ZI-187 and 3IPK, giving a possible explanation for the molecule's ability to inhibit the adhesion of *S. mutans*.

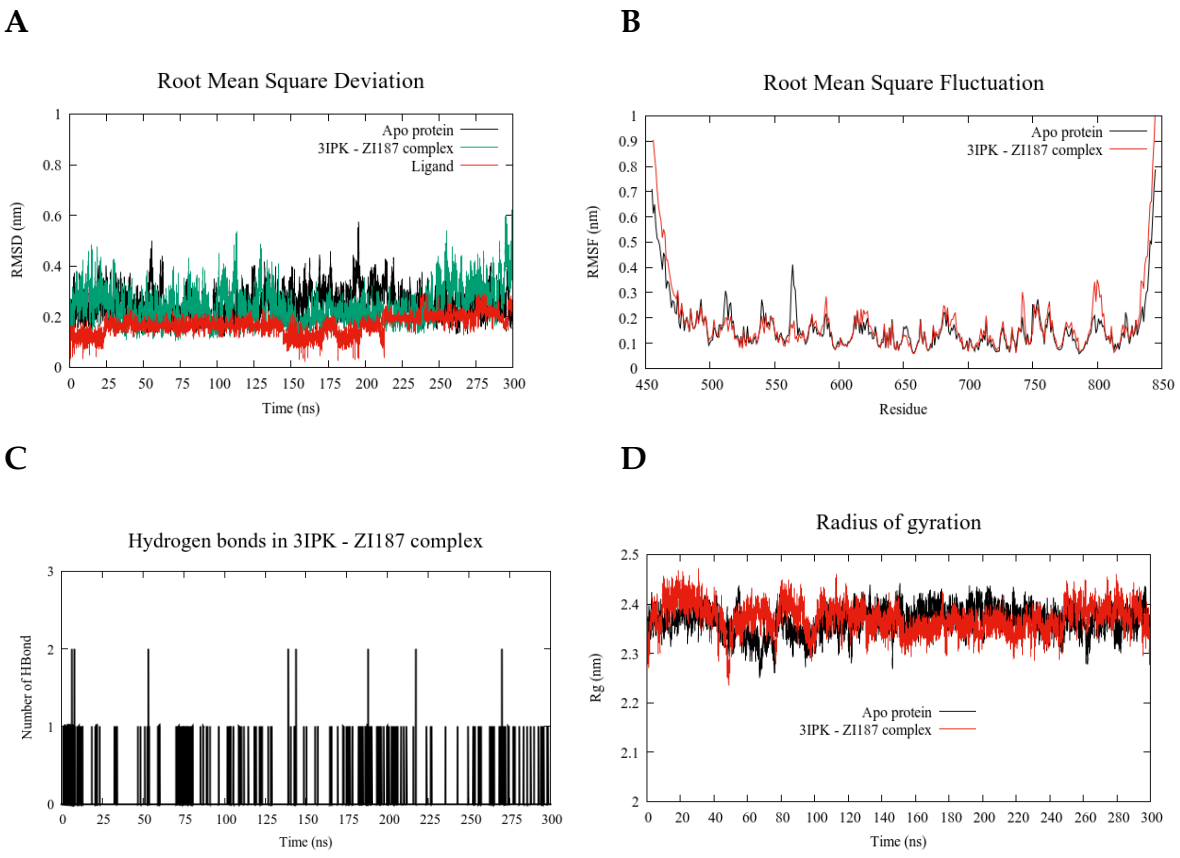

Figure 6. Molecular dynamics simulations analysis. RMSD (Root Mean Square Deviation) (**A**) - RMSF (Root Mean Square Deviation) (**B**), hydrogen bonds (**C**) and Radius of gyration (**D**) calculated for ZI-187/3IPK complex.

Preprints (www.preprints.org) | NOT PEER-REVIEWED | Posted: 16 October 2020 doi:10.20944/preprints202010.0351.v1

Finally, the present work allowed to establish a virtual search strategy and selection pipeline for adhesion inhibitory molecules of a cariogenic bacteria but that could be applicable to any pathogen. This study, to the best of our knowledge, is the first report that uses the *S. mutans* Ag I/II as a target, since the previous studies were mainly performed on Gtfs or sortase A proteins. Three molecules were selected ZI-187, ZI-939 and ZI-906, without showing any cytotoxic effect on periodontal ligament fibroblasts or antimicrobial activity on *S. mutans* or *C. albicans*. However, it is suggested to perform assays in other different human cell lines, as well as on other microorganisms of oral cavity importance to evaluate in a much wider range other possible effects. It was also found, as expected, that the molecules selected had a significant effect in terms of reduction of the *S. mutans* surface adhesion as a single microorganism, but it is very important to carry out complementary studies on multispecies biofilms models, also to identify through transcriptomic analysis if there are variations on the expression of adhesion genes dependent and independent of sucrose when treating bacteria with the selected molecules, as well as genes that participate in cell signaling during the biofilm development process. Similarly, an *in vivo* cariogenic model should be established in order to insight the anti-cariogenic capacity of these molecules.

3. Materials and Methods

3.1 Structure based virtual Screening

3.1.1 Target proteins selection

3D protein structures for the virtual search were selected using the Ag I/II of *S. mutans* sequence AFR75221.1 (NCBI https://www.ncbi.nlm.nih.gov/) and the 3D SWISS-MODEL software (http://swissmodel.expasy.org/). 3D structures of two Ag I/II protein fragments 3IPK (PDB-ID) [18] and 3QE5 [20], were used for a sequence and protein structure similarity analysis using a BLAST-P (Protein Basic Local Alignment Search Tool - NCBI) and the FAT-CAT server (Flexible structure Alignment by Chaining Aligned fragment pairs allowing Twists) [46] to search for similar (rigid) protein structures, using similarities only with a P-value <0.05. Subsequently, for 3IPK and 3QE5 proteins an analysis of binding sites "Pockets" using meta-servers MetaPocket 2.0 [29] and COACH [30] was carried out. 3D structures of the proteins were obtained in PDB format and edited in AutoDockTools 4.0 (http://mgltools.scripps.edu) [47]. Molecular docking of molecules with AgI/II protein fragments, was performed at the Texas Advanced Computing Center (TACC: Texas Advanced Computing Center; Austin, TX) using 3 libraries "ZINC (Lrg)" of ~ 642,759, Library "ZINC (Sm)" of ~ 46,702 molecules, and "ZINC Natural Cmpds (Large)" of 194,090 from the ZINC15 database [48], a total of ~ 883,551 molecules.

3.1.2 Molecules selection:

Two methodologies were used for molecules selection, one according to the molecular docking score and other according to the number of pockets in which molecules interacted, classification of molecules that interacted in most pockets was carried out using a script executed in the R-studio package (Version 1.0.156); ten molecules were arbitrarily selected from each methodology. An *in silico* analysis was performed using the QuikProp application (Version 3.2) from Schrödinger software [49], according to [50] with some modifications, in order to analyze pharmacokinetic profiles such as absorption, distribution, metabolism and excretion (ADME). Molecules that had more than two violations of the Lipinski's Rules and that did not comply with more than two of the standard physical-chemical parameters established by 95% of the known drugs, according to Schrödinger's QuikProp program repositories, were excluded.

For computational toxicity prediction of the molecules, the Protox-II program was used [51], for acute toxicity, hepatotoxicity, cytotoxicity, carcinogenicity, mutagenicity and immunotoxicity. In addition, the molecules lethal dose 50 (LD50) (mg/kg) was calculated and classified according to the

Preprints (www.preprints.org) | NOT PEER-REVIEWED | Posted: 16 October 2020 doi:10.20944/preprints202010.0351.v1

Globally Harmonized System of Classification and Labeling of Chemicals (GHS). For this analysis, chlorhexidine was used as the reference drug, one of the most commonly prescribed antiseptic agents in dentistry; the experimental LD50 values of oral administration in mice of this drug were taken from the Pfizer chlorhexidine technical data sheet [52]. Molecules above class 3 and without any probability of toxicity were selected.

3.1.3 Molecule - protein interaction and solubility analysis

ZINC19835187 (Database code Zinc15), ZINC19924906 and ZINC19924939, (ZI-187, ZI-906 and ZI-939, respectively) were selected and the H-bonding interactions between the molecules and the two protein fragments 3ipk - 3qe5 were identified [53] using Biovia Discovery Studio program [54]. The swissADME web server (http://www.swissadme.ch/) was used to predict water solubility characteristics of the molecules , using a consensus of three methods Log S (ESOL), Log S (Ali) and Log S (SILICOS- IT) [55].

3.2 *In vitro* assays

Three molecules were purchased (ZI-498 was not available for sale) from the MolPort company (https://www.molport.com). Stock solution of the molecules were diluted in 100% DMSO (dimethylsulfoxide) at a concentration of 10^4 µM (ZI-187 (MW = 479.6) = 4796 µg/ml; ZI-906 (MW = 453.6) = 4535, 6 µg/ml; ZI-939 (MW = 470.6) = 4075,9 µg/ml).

3.2.1 Cytotoxicity and antimicrobial assays:

Cytotoxic effects of ZI-187, ZI-906 and ZI-939 on periodontal ligament fibroblast cells (FLP) treated for 24 hours with each molecule was evaluated and analyzed by flow cytometry with propidium iodide (PI), using 100 µM of each molecules and DMSO 1 % . *S. mutans* - Lt11 (UB579 WT) [56] and *C. albicans* NCPF 3179 (NCPF, 1986) were cultured overnight in broth BHI BD® at 37 °C shaking at 250 RPM. The next day, *S. mutans* and *C. albicans* suspension in BHI broth (180 µl/well, OD_{600nm}= 0.1) was seeded into 96-well plates (Costar, Cambridge, MA) with 20 µl of the molecules (concentrations of 1.000, 100, 10, µM. DMSO 10%), as a negative control (death) 0.2% Chlorhexidine digluconate (Farpag®) was used, while the corresponding broth without molecules were used as a positive growth control, as well as those treated with DMSO 10% [57]. After incubation for 24 hours at 37°C shaking at 250 RPM, the absorbance was measured in an Epoch™ Microplate spectrophotometer (BioTek®) (OD_{600nm}), to evaluate cell growth and to establish the minimum inhibitory concentration (MIC)

3.2.2 Adhesion assay:

S. mutans-Lt11 (UB579 WT) was cultured in BHI broth (BD®) overnight at 37 °C shaking at 250 RPMI. The culture medium was discarded and bacteria were washed with phosphate buffer solution (PBS 1X) by centrifugation at 3000 RPM for 10 minutes. Subsequently, bacterial suspension in PBS 1X, OD_{600nm}= 1 was measured using an Epoch™ Microplate spectrophotometer (BioTek®) and 180 µl were inoculated into a 96-well microplate (NEST®, Ref: 701001) with 20 µl of each molecule at 200, 100, 50, 25, 12.5 µM and incubated for three hours at 37 °C shaking at 250 RPM [58]. *S. mutans* SpaP-strain (mutant for AgI/II also called SpaP) and *S. mutans*-Lt11 treated with DMSO 10% were used as control. Plate wells were washed with water and adherent cells were stained by adding 200 µL 0.05% crystal violet for 15 min, washed and measured by absorbance at 600 nm after addition of 30% glacial acetic acid.

3.2.3 Data analysis

All experiments were performed in triplicate and reproduced three separate times. Cell viability percentages were reported as negative % PI ± SEM and analyzed by one-way ANOVA, followed by

 doi:10.20944/preprints202010.0351.v1

a Dunnett's multiple comparison test. In *S. mutans* and *C. albicans* growth and adhesion inhibition analysis, the OD data were normalized to percentages and analyzed using D'Agostino & Pearson omnibus and Shapiro-Wilk normality test; subsequently the nonparametric Kruskal–Wallis test with Dunnett's multiple comparisons against the controls *S. mutans* and *C. albicans* treated with DMSO 10%. Finally, the half maximal inhibitory concentration (IC50) was calculated. GraphPad Prism version 6.0 (GraphPad Software, La Jolla California USA, www.graphpad.com) was used and values of $P < 0.05$ were considered statistically significant.

3.2.4 Scanning Electron Microscopy (SEM):

Surface adhesion assays were performed on Thermo Scientific Nunc Lab-Tek and Lab Tek II Chamber Slides, using *S. mutans* - Lt11 untreated and treated with molecule ZI-187 (100 μM). After incubation for three hours at 37 °C shaking at 250 RPM, each sample was washed three times with PBS 1X , then the samples were fixed with 2,5% glutaraldehyde (0.1M PBS) for 24 hours at 4 °C. Finally, the slides were washed three times with distilled water and dehydrated by immersion in solutions of ascending concentrations of ethanol 70, 90 and 100% (10 minutes each) and dried overnight in a laminar flow cabinet. The samples were covered with gold and visualized using a FEI QUANTA-200TM scanning electron microscope with a variable range acceleration voltage of 1–30 KV.

3.2.5 Molecular dynamics simulations (MD)

MD simulations were carried out using the GROMACS 4.5.5 package [59]. Molecule ZI-187 was docked to the 3IPK protein pocket with the highest binding affinity (P1 by COACH predictor). The ZI-187/3IPK complex and the 3IPK protein in its APO state (reference state), were used as initial coordinates for MD simulations. Finally, both systems were subjected to a 300ns production stage, using a 2fs time step. The equilibrations and productions were carried out using a temperature of 310K (36.85 °C) and a 1 bar pressure. Descriptors such as the RMSD (Root of the mean square deviation), the RMSF (Root of the mean square fluctuation) and hydrogen bonds present in the protein-ligand complex were followed with the tools contained g_rms, g_rmsf and g_hbond, respectively.

Author Contributions:

"Conceptualization, Raul E. Rivera, Nestor I. Cardona and Leonardo Padilla; methodology, Raul E. Rivera, Mayri A. Diaz De Rienzo, Wbeimar Rivera, Sandra M. Morales and Maria C. Martinez; software, Raul E. Rivera, Cristian C. Rocha; validation, Raul E. Rivera, Cristian C. Rocha, Nestor I. Cardona and Leonardo Padilla; formal analysis, Raul E. Rivera, Mayri A. Diaz De Rienzo, Wbeimar Rivera, Sandra M. Morales and Maria C. Martinez; investigation, X.X.; resources, X.X.; data curation, Raul E. Rivera, Cristian C. Rocha, Wbeimar Rivera; writing—original draft preparation, Raul E. Rivera.; writing—review and editing, Raul E. Rivera, Nestor I. Cardona, Wbeimar Rivera, Cristian C. Rocha, Mayri A. Diaz De Rienzo, Sandra M. Morales, Maria C. Martinez. authors have read and agreed to the published version of the manuscript."

Funding: "This research was funded by COLCIENCIAS, grant number 727-2015 "

Acknowledgments: The authors acknowledge the assistance of Mr Paul Gibbons (Liverpool John Moores University), with the SEM experiments; the *S. mutans* strain donation by Dr. Jane Brittan from the Oral Microbiology Laboratory, Bristol School of Dentistry, University of Bristol (UK), Bristol; the script design by Dr. Gladys Elena Salcedo Echeverry and Dr. Aylan Farid Arenas from Research Group and Counseling in Statistics of the University of Quindío.

Conflicts of Interest: "The authors declare no conflict of interest

References

1. Kyu, H.H.; Abate, D.; Abate, K.H.; Abay, S.M.; Abbafati, C.; Abbasi, N.; Abbastabar, H.; Abd-Allah, F.; Abdela, J.; Abdelalim, A.; et al. Global, regional, and national disability-adjusted life-years (DALYs) for 359 diseases and injuries and healthy life expectancy (HALE) for 195 countries and territories, 1990-2017: A systematic analysis for the Global Burden of Disease Study 2017. *Lancet* **2018**, doi:10.1016/S0140-6736(18)32335-3.

2. Vos, T.; Allen, C.; Arora, M.; Barber, R.M.; Brown, A.; Carter, A.; Casey, D.C.; Charlson, F.J.; Chen, A.Z.; Coggeshall, M.; et al. Global, regional, and national incidence, prevalence, and years lived with disability for 310 diseases and injuries, 1990–2015: a systematic analysis for the Global Burden of Disease Study 2015. *Lancet* **2016**, doi:10.1016/S0140-6736(16)31678-6.

3. Lu, M.; Xuan, S.; Wang, Z. Oral microbiota: A new view of body health. *Food Sci. Hum. Wellness* **2019**, *8*, 8–15, doi:10.1016/j.fshw.2018.12.001.

4. Tanzer, J.M. Dental Caries is a Transmissible Infectious Disease: The Keyes and Fitzgerald Revolution. *J. Dent. Res.* **1995**, *74*, 1536–1542, doi:10.1177/00220345950740090601.

5. Selwitz, R.H.; Ismail, A.I.; Pitts, N.B. Dental caries. *Lancet* **2007**, *369*, 51–59, doi:http://dx.doi.org/10.1016/S0140-6736(07)60031-2.

6. Kolenbrander, P.E.; Palmer, R.J.; Periasamy, S.; Jakubovics, N.S. Oral multispecies biofilm development and the key role of cell-cell distance. *Nat. Rev. Microbiol.* **2010**, *8*, 471–480, doi:10.1038/nrmicro2381.

7. Mitchell, T.J. The pathogenesis of streptococcal infections: from Tooth decay to meningitis. *Nat. Rev. Microbiol.* **2003**, *1*, 219–230, doi:10.1038/nrmicro771.

8. Pecharki, D.; Petersen, F.C.; Assev, S.; Scheie, A.A. Involvement of antigen I/II surface proteins in Streptococcus mutans and Streptococcus intermedius biofilm formation. *Oral Microbiol. Immunol.* **2005**, *20*, 366–371, doi:10.1111/j.1399-302X.2005.00244.x.

9. Matsumoto-Nakano, M. Role of Streptococcus mutans surface proteins for biofilm formation. *Jpn. Dent. Sci. Rev.* **2018**, *54*, 22–29, doi:10.1016/j.jdsr.2017.08.002.

10. Ren, Z.; Chen, L.; Li, J.; Li, Y. Inhibition of Streptococcus mutans polysaccharide synthesis by molecules targeting glycosyltransferase activity. **2016**, *1*.

11. Batista, M.T.; Souza, R.D.; Ferreira, E.L.; Robinette, R.; Crowley, P.J.; Rodrigues, J.F.; Jeannine Brady, L.; Ferreira, L.C.S.; Ferreira, R.C.C. Immunogenicity and in vitro and in vivo protective effects of antibodies targeting a recombinant form of the Streptococcus mutans P1 surface protein. *Infect. Immun.* **2014**, *82*, 4978–4988, doi:10.1128/IAI.02074-14.

12. Mayr, L.M.; Fuerst, P. The Future of High-Throughput Screening. *J. Biomol. Screen.* **2008**, *13*, 443–448, doi:10.1177/1087057108319644.

13. Mohs, R.C.; Greig, N.H. Drug discovery and development: Role of basic biological research. *Alzheimer's Dement. Transl. Res. Clin. Interv.* **2017**, *3*, 651–657, doi:10.1016/j.trci.2017.10.005.

14. Sinha, S.; Vohora, D. *Drug Discovery and Development: An Overview*; Elsevier Inc., 2017; ISBN 9780128021033.

15. Barbosa, A.; Romário, D.; Avelar, S.; Gomes, G.; Albuquerque, A.R.; Gaudencio, T. In Silico Approach for the Identification of Potential Targets and Specific Antimicrobials for Streptococcus mutans. *Adv Biosci Biotech* **2014**, *5*, 373–385.

16. Ren, Z.; Cui, T.; Zeng, J.; Chen, L.; Zhang, W.; Xu, X.; Cheng, L.; Li, M.; Li, J.; Zhou, X.; et al. Molecule targeting glucosyltransferase inhibits Streptococcus mutans biofilm formation and virulence. *Antimicrob. Agents Chemother.* **2016**, *60*, 126–135, doi:10.1128/AAC.00919-15.

17. Zhang, Q.; Nijampatnam, B.; Hua, Z.; Nguyen, T.; Zou, J.; Cai, X.; Michalek, S.M.; Velu, S.E.; Wu, H. Structure-Based Discovery of Small Molecule Inhibitors of Cariogenic Virulence. *Sci. Rep.* **2017**, *7*, 1–10, doi:10.1038/s41598-017-06168-1.

18. Larson, M.R.; Rajashankar, K.R.; Patel, M.H.; Robinette, R.A.; Crowley, P.J.; Michalek, S.; Brady, L.J.; Deivanayagam, C. Elongated fibrillar structure of a streptococcal adhesin assembled by the high-affinity association of alpha- and PPII-helices. *Proc. Natl. Acad. Sci. U. S. A.* **2010**, *107*, 5983–8, doi:10.1073/pnas.0912293107.

19. Troffer-Charlier, N.; Ogier, J.; Moras, D.; Cavarelli, J. Crystal structure of the V-region of streptococcus mutans antigen I/II at 2.4 Å resolution suggests a sugar preformed binding site. *J. Mol. Biol.* **2002**, *318*, 179–188, doi:10.1016/S0022-2836(02)00025-6.

20. Larson, M.R.; Rajashankar, K.R.; Crowley, P.J.; Kelly, C.; Mitchell, T.J.; Brady, L.J.; Deivanayagam, C. Crystal structure of the C-terminal region of Streptococcus mutans antigen I/II and characterization of salivary agglutinin adherence domains. *J. Biol. Chem.* **2011**, *286*, 21657–21666, doi:10.1074/jbc.M111.231100.

21. Nylander, Å.; Forsgren, N.; Persson, K. Structure of the C-terminal domain of the surface antigen SpaP from the caries pathogen Streptococcus mutans. *Acta Crystallogr. Sect. F Struct. Biol. Cryst. Commun.* **2011**, *67*, 23–26, doi:10.1107/S174430911004443X.

22. Miyanohara, M.; Imai, S.; Okamoto, M.; Saito, W.; Nomura, Y.; Momoi, Y.; Tomonaga, M.; Hanada, N. Distribution of Streptococcus troglodytae and Streptococcus dentirousetti in chimpanzee oral cavities. *Microbiol. Immunol.* **2013**, *57*, 359–365, doi:10.1111/1348-0421.12047.

23. Zhang, M.; Yan, L.; Zhu, G.; Holifield, M.; Todd, D.; Zhang, S. Streptococcus troglodytidis sp. nov., isolated from a foot abscess of a chimpanzee (Pan troglodytes). *Int. J. Syst. Evol. Microbiol.* **2013**, *63*, 449–453, doi:10.1099/ijs.0.038133-0.

24. Cristensen, J.J.; Facklam, R.R. Granulicatella and Abiotrophia species from human clinical specimens. *J. Clin. Microbiol.* **2001**, *39*, 3520–3523, doi:10.1128/JCM.39.10.3520-3523.2001.

25. Copeland, A.; Sikorski, J.; Lapidus, A.; Nolan, M.; Del Rio, T.G.; Lucas, S.; Chen, F.; Tice, H.; Pitluck, S.; Cheng, J.F.; et al. Complete genome sequence of Atopobium parvulum type strain (IPP 1246 T). *Stand. Genomic Sci.* **2009**, *1*, 166–173, doi:10.4056/sigs.29547.

26. Heim, K.P.; Crowley, P.J.; Long, J.R.; Kailasan, S.; McKenna, R.; Brady, L.J. An intramolecular lock facilitates folding and stabilizes the tertiary structure of streptococcus mutans adhesin p1. *Proc. Natl. Acad. Sci. U. S. A.* **2014**, *111*, 15711–15716, doi:10.1073/pnas.1413018111.

27. Lionta, E.; Spyrou, G.; Vassilatis, D.K.; Cournia, Z. Send Orders for Reprints to reprints@benthamscience.net Structure-Based Virtual Screening for Drug Discovery: Principles, Applications and Recent Advances. *Curr. Top. Med. Chem.* **2014**, *14*, 1923–1938, doi:10.2174/1568026614666140929124445.

28. Gazgalis, D.; Zaka, M.; Zaka, M.; Abbasi, B.H.; Logothetis, D.E.; Mezei, M.; Cui, M. Protein Binding Pocket Optimization for Virtual High-Throughput Screening (vHTS) Drug Discovery. *ACS Omega* **2020**, *5*, 14297–14307, doi:10.1021/acsomega.0c00522.

29. Huang, B. MetaPocket: A Meta Approach to Improve Protein Ligand Binding Site Prediction. *Omi. A J. Integr. Biol.* **2009**, *13*, 325–330, doi:10.1089/omi.2009.0045.

30. Yang, J.; Roy, A.; Zhang, Y. Protein-ligand binding site recognition using complementary binding-specific substructure comparison and sequence profile alignment. *Bioinformatics* **2013**, *29*, 2588–2595, doi:10.1093/bioinformatics/btt447.

31. Hadži, D.; Kidrič, J.; Koller, J.; Mavri, J. The role of hydrogen bonding in drug-receptor interactions. *J. Mol. Struct.* **1990**, *237*, 139–150, doi:10.1016/0022-2860(90)80136-8.

32. Kuhn, B.; Mohr, P.; Stahl, M. Intramolecular hydrogen bonding in medicinal chemistry. *J. Med. Chem.* **2010**, *53*, 2601–2611, doi:10.1021/jm100087s.

33. Caron, G.; Kihlberg, J.; Ermondi, G. Intramolecular hydrogen bonding: An opportunity for improved design in medicinal chemistry. *Med. Res. Rev.* **2019**, *39*, 1707–1729, doi:10.1002/med.21562.

34. J. R. Yunta, M. It Is Important to Compute Intramolecular Hydrogen Bonding in Drug Design? *Am. J. Model. Optim.* **2017**, *5*, 24–57, doi:10.12691/ajmo-5-1-3.

35. Ermondi, G.; Caron, G. Why we need to implement intramolecular hydrogen-bonding considerations in drug discovery. *Future Med. Chem.* **2016**, *31*, 48–49.

36. Cottet-Rousselle, C.; Ronot, X.; Leverve, X.; Mayol, J.F. Cytometric assessment of mitochondria using fluorescent probes. *Cytom. Part A* **2011**, *79 A*, 405–425, doi:10.1002/cyto.a.21061.

37. Rieger, A.M.; Nelson, K.L.; Konowalchuk, J.D.; Barreda, D.R. Modified annexin V/propidium iodide apoptosis assay for accurate assessment of cell death. *J. Vis. Exp.* **2011**, 3–6, doi:10.3791/2597.

38. Scharnow, A.M.; Solinski, A.E.; Wuest, W.M. Targeting: S. mutans biofilms: A perspective on preventing dental caries. *Medchemcomm* **2019**, *10*, 1057–1067, doi:10.1039/c9md00015a.

39. Wang, J.; Shi, Y.; Jing, S.; Dong, H.; Wang, D.; Wang, T. Astilbin Inhibits the Activity of Sortase A from Streptococcus mutans. *Molecules* **2019**, *24*, 465, doi:10.3390/molecules24030465.

40. Luo, H.; Liang, D.F.; Bao, M.Y.; Sun, R.; Li, Y.Y.; Li, J.Z.; Wang, X.; Lu, K.M.; Bao, J.K. In silico identification of potential inhibitors targeting Streptococcus mutans sortase A. *Int. J. Oral Sci.* **2017**, *9*, 53–62, doi:10.1038/ijos.2016.58.

41. Hu, P.; Huang, P.; Chen, M.W. Curcumin reduces Streptococcus mutans biofilm formation by inhibiting sortase A activity. *Arch. Oral Biol.* **2013**, *58*, 1343–1348, doi:10.1016/j.archoralbio.2013.05.004.

42. Burgos-Morón, E.; Calderón-Montaño, J.M.; Salvador, J.; Robles, A.; López-Lázaro, M. The dark side of curcumin Estefanı´a. *Int. J. Cancer* **2010**, *126*, 1771–1775, doi:10.1038/s41567-018-0261-2.

43. Cianfruglia, L.; Minnelli, C.; Laudadio, E.; Scirè, A.; Armeni, T. Side effects of curcumin: Epigenetic and antiproliferative implications for normal dermal fibroblast and breast cancer cells. *Antioxidants* **2019**, *8*, 1–13, doi:10.3390/antiox8090382.

44. Huang, P.; Hu, P.; Zhou, S.Y.; Li, Q.; Chen, W.M. Morin inhibits sortase A and subsequent biofilm formation in streptococcus mutans. *Curr. Microbiol.* **2014**, *68*, 47–52, doi:10.1007/s00284-013-0439-x.

45. Yang, J.Y.; Lee, H.S. Evaluation of antioxidant and antibacterial activities of morin isolated from mulberry fruits (Morus alba L.). *J. Korean Soc. Appl. Biol. Chem.* **2012**, *55*, 485–489, doi:10.1007/s13765-012-2110-9.

46. Ye, Y.; Godzik, A. FATCAT: A web server for flexible structure comparison and structure similarity searching. *Nucleic Acids Res.* **2004**, *32*, 582–585, doi:10.1093/nar/gkh430.

47. Morris, G.M.; Huey, R.; Lindstrom, W.; Sanner, M.F.; Belew, R.K.; Goodsell, D.S.; Olson, A.J. AutoDock4 and AutoDockTools4: Automated docking with selective receptor flexibility. *J. Comput. Chem.* **2009**, *30*, 2785–91, doi:10.1002/jcc.21256.

48. Sterling, T.; Irwin, J.J. ZINC 15 - Ligand Discovery for Everyone. *J. Chem. Inf. Model.* **2015**, *55*, 2324–2337, doi:10.1021/acs.jcim.5b00559.

49. Schrödinger Schrödinger Release 2018-1. *Maest. Interoperability Tools, Desmond Mol. Dyn. Syst.* 2018.

50. Rivera-Pérez, W.A.; Yépes-Pérez, A.F.; Martínez-Pabón, M.C. Molecular docking and in silico studies of the physicochemical properties of potential inhibitors for the phosphotransferase system of Streptococcus mutans. *Arch. Oral Biol.* **2019**, *98*, 164–175, doi:10.1016/j.archoralbio.2018.09.020.

51. Banerjee, P.; Eckert, A.O.; Schrey, A.K.; Preissner, R. ProTox-II: A webserver for the prediction of toxicity of chemicals. *Nucleic Acids Res.* **2018**, *46*, W257–W263, doi:10.1093/nar/gky318.

52. Pfizer Inc *Material Safety Data Sheet Material Safety Data Sheet*; 2012;

53. Chen, D.; Oezguen, N.; Urvil, P.; Ferguson, C.; Dann, S.M.; Savidge, T.C. Regulation of protein-ligand binding affinity by hydrogen bond pairing. *Sci. Adv.* **2016**, *2*, doi:10.1126/sciadv.1501240.

54. BIOVIA, D. Discovery Studio Modeling Environment, Release 2017, San Diego: DassaultSystèmes, 2016. *Adres http//accelrys. com/products/collaborative-science/biovia-discoverystudio/visualization download. php*

2016.

55. Daina, A.; Michielin, O.; Zoete, V. SwissADME: A free web tool to evaluate pharmacokinetics, drug-likeness and medicinal chemistry friendliness of small molecules. *Sci. Rep.* **2017**, *7*, 1–13, doi:10.1038/srep42717.

56. Tao, L.; Tanzer, J.M.; MacAlister, T.J.; Tao, L.; Tanzer, J.M. Transformation Efficiency of EMS-induced Mutants of Streptococcus mutans of Altered Cell Shape. *J. Dent. Res.* **1993**, *72*, 1032–1039, doi:10.1177/00220345930720060701.

57. Chen, L.; Jia, L.; Zhang, Q.; Zhou, X.; Liu, Z.; Li, B.; Zhu, Z.; Wang, F.; Yu, C.; Zhang, Q.; et al. A novel antimicrobial peptide against dental-caries-associated bacteria. *Anaerobe* **2017**, *47*, 165–172, doi:10.1016/j.anaerobe.2017.05.016.

58. Esberg, A.; Sheng, N.; Mårell, L.; Claesson, R.; Persson, K.; Borén, T.; Strömberg, N. EBioMedicine Streptococcus Mutans Adhesin Biotypes that Match and Predict Individual Caries Development. *EBioMedicine* **2017**, *24*, 205–215, doi:10.1016/j.ebiom.2017.09.027.

59. Van Der Spoel, D.; Lindahl, E.; Hess, B.; Groenhof, G.; Mark, A.E.; Berendsen, H.J.C. GROMACS: Fast, flexible, and free. *J. Comput. Chem.* **2005**, *26*, 1701–1718, doi:10.1002/jcc.20291.